

## RESEARCH ARTICLE

# Deciphering the Intricate Control of Minerals on Deep Soil Carbon Stability and Persistence in Alaskan Permafrost

Yi-Xuan Guo<sup>1</sup>  | Guang-Hui Yu<sup>1</sup>  | Shuijin Hu<sup>2</sup>  | Chao Liang<sup>3</sup>  | Andreas Kappler<sup>4</sup>  | Mark Torre Jorgenson<sup>5</sup>  | Laodong Guo<sup>6</sup>  | Georg Guggenberger<sup>7</sup> 

<sup>1</sup>Tianjin Key Laboratory of Earth Critical Zone Science and Sustainable Development in Bohai Rim, Institute of Surface-Earth System Science, School of Earth System Science, Tianjin University, Tianjin, People's Republic of China | <sup>2</sup>Department of Entomology and Plant Pathology, North Carolina State University, Raleigh, North Carolina, USA | <sup>3</sup>Key Laboratory of Forest Ecology and Management, Institute of Applied Ecology, Chinese Academy of Sciences, Shenyang, People's Republic of China | <sup>4</sup>Cluster of Excellence: EXC 2124: Controlling Microbes to Fight Infections, Geomicrobiology, Center for Applied Geosciences, University of Tübingen, Tübingen, Germany | <sup>5</sup>Alaska Ecoscience, Fairbanks, Alaska, USA | <sup>6</sup>School of Freshwater Sciences, University of Wisconsin-Milwaukee, Milwaukee, Wisconsin, USA | <sup>7</sup>Soil Sciences Section, Institute of Earth System Sciences, Leibniz University, Hannover, Germany

**Correspondence:** Guang-Hui Yu ([yuguanghui@tju.edu.cn](mailto:yuguanghui@tju.edu.cn))

**Received:** 29 August 2024 | **Revised:** 6 October 2024 | **Accepted:** 8 October 2024

**Funding:** This work was supported by National Natural Science Foundation of China, 32241037, 41977271, U22A20608. Tianjin Municipal Science and Technology Program, 23ZYJDC00050, 24ZYJDC00330.

**Keywords:** microbial necromass | microbial residues | mineral binding sites | nanozyme | permafrost | peroxidase | reactive minerals | soil carbon accrual | synchrotron radiation |  $\mu$ -FTIR

## ABSTRACT

Understanding the fate of organic carbon in thawed permafrost is crucial for predicting climate feedback. While minerals and microbial necromass are known to play crucial roles in the long-term stability of organic carbon in subsoils, their exact influence on carbon persistence in Arctic permafrost remains uncertain. Our study, combining radiocarbon dating and biomarker analyses, showed that soil organic carbon in Alaskan permafrost had millennial-scale radiocarbon ages and contained only 10%–15% microbial necromass carbon, significantly lower than the global average of ~30%–60%. This ancient carbon exhibited a weak correlation with reactive minerals but a stronger correlation with mineral weathering (reactive iron to total iron ratio). Peroxidase activity displayed a high correlation coefficient ( $p < 10^{-6}$ ) with  $\Delta^{14}\text{C}$  and  $\delta^{13}\text{C}$ , indicating its strong predictive power for carbon persistence. Further, a positive correlation between peroxidase activity and polysaccharides indicates that increased peroxidase activity may promote the protection of plant residues, potentially by fostering the formation of mineral-organic associations. This protective role of mineral surfaces on biopolymers was further supported by examining 1451 synchrotron radiation infrared spectra from soil aggregates, which revealed a strong correlation between mineral OH groups and organic functional groups at the submicron scale. An incubation experiment revealed that increased moisture contents, particularly within the 0%–40% range, significantly elevated peroxidase activity, suggesting that ancient carbon in permafrost soils is vulnerable to moisture-induced destabilization. Collectively, this study offers mechanistic insights into the persistence of carbon in thawed permafrost soils, essential for refining permafrost carbon-climate feedbacks.

## 1 | Introduction

Understanding the fate of carbon (C) in thawed permafrost is crucial for accurately predicting climate feedback. Despite covering only 16% of Earth's land area, permafrost contributes approximately 50% of the soil organic C stock in frozen ground (Schuur et al. 2022; Turetsky et al. 2020). This reservoir, vulnerable to climate change-induced thawing, is projected to release 67–237 Pg of C by 2100, based on model-data synthesis under medium and high emission scenarios (Schuur et al. 2022). Considering a stronger plant C uptake response than that obtained in earlier Coupled Model Intercomparison Project (CMIP) 5 studies, it is estimated to emit 26 Pg C by 2100 under RCP8.5 (McGuire et al. 2018). Consequently, these regions are considered potential climate “tipping elements” (Armstrong McKay et al. 2022; Lenton et al. 2008). Concerns about its vulnerability to microbial decomposition in a changing world emphasize the need to understand the accumulation (i.e., amount) and persistence (i.e., turnover time or the mean system “age”) of C in soils (Sierra et al. 2018). Recent research indicates that the interplay between microbial properties, mineral variables, and climatic conditions plays a crucial role in influencing soil C persistence (Cotrufo and Lavalley 2022; Doetterl et al. 2015). The contemporary paradigm posits that soil microbes efficiently process labile plant carbon into microbial necromass (cell residues) that tend to attach on mineral surfaces and form mineral-associated organic C (hereafter the “necromass stabilization mechanism”) (Cotrufo et al. 2013; Kleber et al. 2015; Mikutta et al. 2019; Luo et al. 2021; Sokol and Bradford 2018; Wang et al. 2024). This paradigm, however, has primarily been tested in temperate and tropical soils (Hall and Silver 2013; Koegel-Knabner et al. 2008; Kramer and Chadwick 2018), and its application to permafrost soils, particularly in their subsoils (30–200 cm depth), remains challenging.

The challenge is mainly derived from the unusual properties of organic matter (OM) and minerals in Arctic permafrost soils. These soils contain a high proportion of vulnerable particulate OM (García-Palacios et al. 2024; Prater et al. 2020). Compared to undecomposed organic residues from tundra-steppe vegetation that has not undergone microbial decomposition (Martens et al. 2023), microbial necromass, representing the C pool from microbial remnants (Liang et al. 2019), may exhibit distinct responses to permafrost thawing. This holds particularly true for subsoil horizons of permafrost soils, where approximately 70% of whole soil organic C (SOC) is located (Jackson et al. 2017). To date, research on microbial necromass in Arctic permafrost subsoils is scarce (Dai et al. 2002) compared to other permafrost areas such as the Tibetan Plateau (He et al. 2022), despite its potential pivotal contribution to global C cycles.

The degradation and stabilization of soil OM (SOM) components, such as necromass, are thought to be influenced by microbial community structure and mineral reactivity, with the former impacting its degradation while the latter affecting its sorptive preservation in soils (Buckeridge, Creamer, and Whitaker 2022; Xiao et al. 2023). In the Arctic permafrost soils, colder temperatures may favor fungal dominance due to their less substrate-limited nature (Gavazov et al. 2022). Many fungi also have strong capability at producing peroxidases that can break down recalcitrant OM (Sinsabaugh 2010; Tian and Shi 2014). Key peroxidases, such as lignin peroxidase and manganese peroxidase, play crucial roles in

ecosystem processes like lignin degradation and C mineralization (Sinsabaugh 2010). Emerging evidence suggests that fungi contribute to SOM persistence through rapid litter decomposition and the formation of mineral-organic associations on fresh litter surfaces (Witzgall et al. 2021). Using isotopic labelling and nanoscale secondary ion mass spectrometry (NanoSIMS) imaging, researchers demonstrated that litter surfaces act as a nucleus for stable SOC formation (Witzgall et al. 2021), suggesting an alternative mechanism to sorptive preservation in permafrost soils. An incubation study with <sup>44</sup>Ca-labeled soils and <sup>13</sup>C<sup>15</sup>N-labeled leaf litter, supported by NanoSIMS images, further confirmed the formation of mineral-microbial product associations on litter surfaces (Shabtai et al. 2023). Such mineral-protected SOM is affected by mineral reactivity (Koegel-Knabner et al. 2008; Mikutta et al. 2019; Xiao et al. 2023). However, Arctic permafrost subsoils are composed of minerals with low reactivity (low content of secondary phyllosilicate clay minerals and (oxyhydr)oxides) (Ping et al. 2015), suggesting that the formation of mineral-organic complexes may be less important for SOC accrual and persistence compared to soils of the temperate regions. Consequently, microbial-derived peroxidases, particularly from fungi, may play a crucial yet underexplored role in SOC stabilization in Arctic permafrost.

In this work, we hypothesize that mineral attachment, induced by peroxidase degradation, facilitates carbon stabilization in permafrost soils. This proposed hypothesis posits that microbial-produced peroxidases can degrade SOC to create etching sites, which subsequently enhances the accrual and persistence of SOC through mineral attachment in permafrost regions. To test this hypothesis, we employ a colorimetric reaction method to assess peroxidase activities (Jiang et al. 2018). Given that peroxidases use hydrogen peroxide (H<sub>2</sub>O<sub>2</sub>) as the electron acceptor, we utilize the titanium sulfate method (Satterfield and Bonnell 1955) to evaluate the contents of H<sub>2</sub>O<sub>2</sub>, a widespread oxidant in permafrost soils (Page et al. 2013; Trusiak et al. 2018). Considering the differences in OM compositions, we use selective extraction methods (Mehra and Jackson 1958) and amino sugar biomarkers (Hu et al. 2024; Liang et al. 2019) to determine mineral-associated-organic carbon (OC) and microbial necromass, respectively. Since microbial necromass stabilization involves not only amino sugars but also other biopolymers (Buckeridge, Creamer, and Whitaker 2022; Hall et al. 2020), we utilize correlative synchrotron radiation infrared (IR) and micro-X-ray fluorescence (μ-XRF) spectromicroscopy to investigate the in situ correlation between minerals and microbial- and plant-derived biopolymers in soil aggregates (Kang et al. 2024; Lehmann, Kinyangi, and Solomon 2007; Wasner et al. 2024). Our study aims to: (1) investigate the contribution of microbial necromass to SOC in Alaskan permafrost subsoils and (2) explore the mechanisms of SOC stabilization and persistence driven by peroxidase activity.

## 2 | Materials and Methods

### 2.1 | Soil Sampling

Permafrost cores were collected from depths ranging from 56 cm to 310 cm at three sites in Alaska: Barrow, Creamers Field, and Jago, between 2011 and 2019 (Figure 1 and Figure S5). In Barrow, the ecosystem was moist-shrub tundra, while in Creamers Field, it was characterized as birch forest. In

Jago, the ecosystems were characterized as moist sedge-dryas tundra (one site) and tussock tundra, respectively. The prevalent regional soil types encompass primarily Gelisols according to USDA Soil Taxonomy, alongside lesser occurrences of aquents, fluvents, and cryepts (Ping et al. 2015). A total of four soil cores, comprising eight individual soil samples, were procured from these three sites. The soils were further categorized into two depth ranges (Behnke et al. 2023): upper (56–69 cm) and deeper (144–310 cm) layers (Table 1). Details about sites and soil properties are provided in Tables S3–S5, Data S1, and retrieved from the database in the Web site: <https://northslope.science.org/catalog/>. Subsequently, the subsoils underwent a series of preparations, including grinding using a mortar and pestle, sieving through a 100-mesh sieve, and air-drying.

## 2.2 | Microbial Necromass Assay

We analyzed four amino sugars in permafrost soils, following a modified procedure based on Liang et al. (2019). This analysis involved examining muramic acid (MurA), glucosamine (GluN), galactosamine, and mannosamine via gas chromatography after converting them to aldonitrile acetates. Approximately 1 g of finely ground, air-dried soils underwent hydrolysis with 6 M HCl at 105°C for 8 h to release the amino sugar monomers. Post purification and derivatization, the extracts underwent analysis using a gas chromatograph (GC-2014C, Shimadzu, Japan) fitted with a DB-5 column (60 m × 0.25 mm × 0.25 μm). Identification of individual amino sugar derivatives was carried out by comparing their retention time with authentic standards. Quantification, based on peak areas, was expressed as mass per mass of soil (μg g<sup>-1</sup>) relative to the internal standard myo-inositol, added to the samples' pre-purification.

As a constituent of bacterial cell wall peptidoglycan, MurA is not produced by eukaryotic cells. Although bacterial peptidoglycan contains both MurA and GluN, in soils, GluN is mainly derived from fungal chitin rather than bacterial peptidoglycan (Amelung

et al. 2001). The origin of galactosamine or mannosamine is presently under debate. The calculation of fungal and bacterial necromass C followed Appuhn and Joergensen (2006) with the revision by Engelking, Flessa, and Joergensen (2007) [equations (Eqs.) (1) and (2)]:

$$F - \text{necromass C} = (\text{GluN}/179.17 - 2 \times \text{MurA}/251.23) \times 179.17 \times 9 \quad (1)$$

$$B - \text{necromass C} = \text{MurA} \times 45 \quad (2)$$

where the coefficients 179.17 and 251.23 correspond to the molecular weights of GluN and MurA, respectively. The factor 9 denotes the conversion of fungal GluN to fungal necromass C, while 45 represents the conversion of MurA to bacterial necromass C. The collective microbial necromass C was computed by summing fungal and bacterial necromass C. The ratio of microbial necromass C to SOC signifies the contribution of microbial necromass to SOC.

Most recently, Hu et al. (2024) introduced updated equations (Equations 3 and 4) for calculating fungal and bacterial necromass C:

$$F - \text{necromass C} = (\text{GluN} - 1.16 \times \text{MurA}) \times 10.8, \quad (3)$$

$$B - \text{necromass C} = \text{MurA} \times 31.3. \quad (4)$$

To validate the contribution of microbial necromass C to SOC, these equations (Equations 3 and 4) were compared with earlier ones (Equations 1 and 2) in this study.

## 2.3 | Data Synthesis of Microbial Necromass in Global Soils

To determine the total necromass C ratio in SOC, we conducted a comprehensive data retrieval of microbial necromass data by

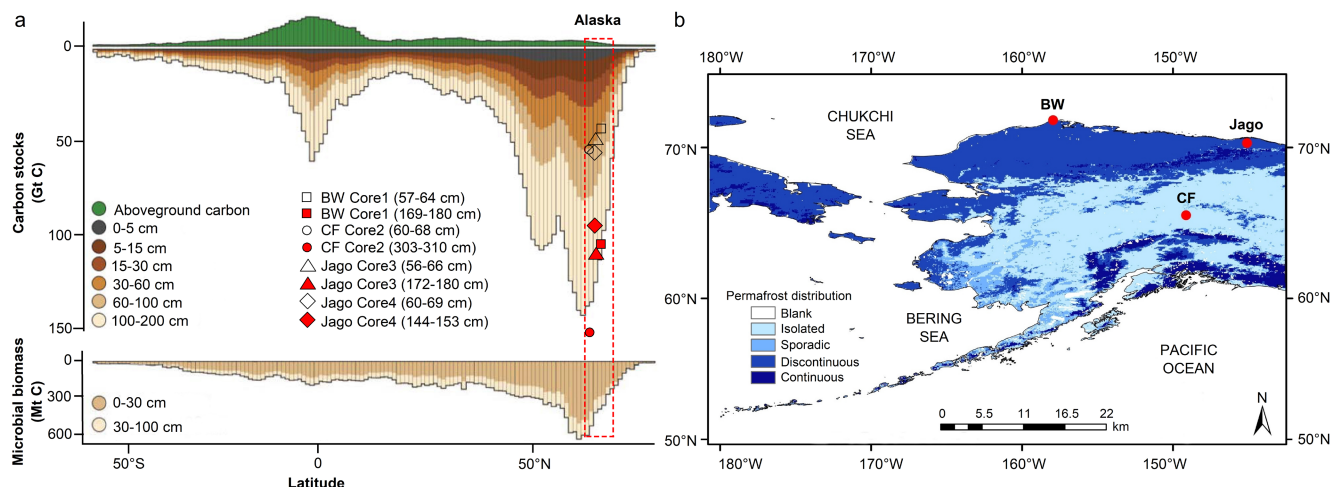


**FIGURE 1** | Carbon stocks and geographic distribution of study sites in Alaska, USA. (a) This illustration shows the latitudinal distribution of organic matter in various terrestrial ecosystems, adapted from Crowther et al. (2019), underscoring the significance of Alaskan permafrost subsoils. (b) Overview map highlighting the study sites, indicating the precise locations of the permafrost drill cores using red markers. A total of eight permafrost soil samples from four different soil cores were gathered from Barrow (BW), Creamers Field (CF), and Jago near Fairbanks in Alaska. Map lines delineate study areas and do not necessarily depict accepted national boundaries.

TABLE 1 | Properties of permafrost soils in Alaska, USA.<sup>a</sup>

Location	Soil core	Depth (cm)	SOC (g kg <sup>-1</sup> )	Fe-bound OC (%)	F-necromass C (g kg <sup>-1</sup> )	B-necromass C (g kg <sup>-1</sup> )	Δ <sup>14</sup> C (‰)	Age (yr BP)	Water-extracted Fe (mg kg <sup>-1</sup> )	Fe <sub>DCB</sub> (g kg <sup>-1</sup> )	SRO (g kg <sup>-1</sup> )	Fe <sub>DCB</sub> /Fe <sub>t</sub>
Barrow	Core 1	57–64	37.4 ± 1.2	12.5 ± 0.5	3.4 ± 0.2	1.8 ± 0.1	-339.3	3329	58.1 ± 5.4	2.5 ± 0.4	6.7 ± 0.2	0.07
		169–180	112 ± 6.3	32.7 ± 2.6	8.9 ± 0.3	2.7 ± 0.2	-570.3	6785	52.0 ± 1.5	3.4 ± 0.2	3.5 ± 0.2	0.12
Creamers Field	Core 2	60–68	23.6 ± 0.4	23.0 ± 4.1	2.9 ± 0.0	0.6 ± 0.0	-579.3	6954	5.6 ± 0.9	1.9 ± 0.1	2.0 ± 0.0	0.04
		303–310	2.3 ± 0.1	15.2 ± 0.9	0.4 ± 0.0	0.1 ± 0.0	-839.4	14,693	12.9 ± 3.7	4.1 ± 0.0	3.9 ± 0.1	0.08
Jago	Core 3	56–66	55.1 ± 0.1	19.9 ± 3.3	4.3 ± 0.1	1.5 ± 0.2	-318.4	3078	28.6 ± 3.8	3.9 ± 0.1	4.7 ± 0.1	0.11
		172–180	30.7 ± 0.1	16.0 ± 1.9	2.3 ± 0.0	0.7 ± 0.0	-486.5	5353	27.5 ± 2.9	2.1 ± 0.1	2.9 ± 0.0	0.07
Core 4	Core 4	60–69	32.9 ± 0.5	6.5 ± 1.3	3.7 ± 0.1	1.2 ± 0.0	-342.3	3366	39.2 ± 1.6	6.2 ± 0.4	7.7 ± 0.3	0.14
		144–153	127 ± 2.0	20.4 ± 4.7	13.1 ± 0.2	4.1 ± 0.0	-561.3	6618	12.1 ± 0.6	4.6 ± 0.1	4.8 ± 0.1	0.11

<sup>a</sup>Note that measurements for Δ<sup>14</sup>C, Fe<sub>t</sub>, and Fe<sub>DCB</sub>/Fe<sub>t</sub> were conducted without replication. The other index values are presented as means derived from three replicates along with their corresponding standard error (SE). SOC, soil organic carbon. F-necromass, fungal necromass; B-necromass, bacterial necromass; Fe<sub>DCB</sub> and Fe-bound OC denote the reactive iron oxide and fraction of organic carbon (OC) associated with reactive minerals, respectively. SRO stands for short-range-ordered (SRO) minerals extracted via the acid oxalate method. Fe<sub>t</sub> (total Fe) is determined using X-ray fluorescence spectrometry. Fe<sub>DCB</sub>/Fe<sub>t</sub> denotes the degree of mineral weathering. Water-extracted Fe is quantified using ICP-OES after shaking extraction with water (soil-water ratio 1:5) (Data S1).

searching keywords “microbial necromass”, “amino sugar”, “fungal necromass”, “bacterial necromass”, and “microbial residue” from Web of Science (<http://apps.webofknowledge.com/>). Our data collection process comprised the following steps: (1) Directly gathering data values for the quantities of four amino sugars (GluN, galactosamine, MurA, and mannosamine) individually, alongside their cumulative sum; (2) in scenarios where specific mannosamine data were absent, we utilized the sum of the other three types; (3) converting data related to fungal residual C and bacterial residual C into GluN and MurA content by using the provided conversion coefficients (Equations 1 and 2); (4) standardizing the diverse units extracted from the literatures as a unified expression: (B-necromass C + F-necromass C)/SOC (%); and (5) collecting sampling details such as latitude and longitude from the studies. This meticulous data gathering process resulted in the construction of a comprehensive microbial necromass database sourced from 126 published papers. This database encompasses 980 observations of microbial necromass spanning the period from 1996 to 2023, derived from soil samples worldwide. The detailed dataset is available in Data S2.

## 2.4 | Peroxidase Activity Assay

We introduced a colorimetric approach (Jiang et al. 2018) to determine the peroxidase activity in the soils. Two milligrams of soil was mixed with 1 mL of the test 3,3',5,5'-tetramethylbenzidine (TMB) solution in 0.2 M NaAc-HAc buffer (pH 3.6). Following the addition of H<sub>2</sub>O<sub>2</sub> (to reach a final concentration of 50 mM) at 37°C, a blue color developed. Using a SpectraMax M5 spectrophotometer (Molecular Devices, Sunnyvale, CA), absorbance reading was taken at 652 nm every 25 s for a duration of 30 min. A control was included without the addition of H<sub>2</sub>O<sub>2</sub> or the TMB solution. The peroxidase activity of the soils was calculated using Equation (5):

$$\text{Peroxidase activity} = V / (\epsilon \times l) \times (\Delta A / \Delta t) / [m], \quad (5)$$

where peroxidase activity (U g<sup>-1</sup>) represents the amount of soil capable of catalytically producing 1 μM of product per minute per gram at 37°C; V denotes the total volume of the reaction solution (μL); ε signifies the molar absorption coefficient of the substrate (39,000 M<sup>-1</sup> cm<sup>-1</sup>); l indicates the path length of light propagation (cm); ΔA represents the absorbance after subtracting the blank value; and ΔA/Δt stands for the initial rate of absorbance change at 652 nm (min<sup>-1</sup>); and [m] denotes the weight (g) of the soil. The detailed dataset is available in Data S3.

To ascertain that the detected peroxidase activity originated from the soils rather than water-extracted iron ions, we subjected the soils to cultivation in a standard reaction solution (pH 3.6, NaAc-HAc buffer) at 37°C for 400 s, the necessary duration for activity measurement. Subsequently, the soils were separated from the solution through centrifugation at 10,000g. We then conducted a comparative analysis between the activity of the solution and that of the collected soils under identical conditions to validate our observations.

## 2.5 | Correlative Synchrotron Infrared Spectromicroscopy and $\mu$ -XRF Analysis

To assess the spatial correlation between structural OH in minerals and plant- and microbial-derived biopolymers, we conducted an in situ assessment of permafrost soil aggregates using  $\mu$ -XRF and synchrotron radiation-based IR spectromicroscopy. To achieve this, we manually selected from the eight soil samples intact soil macro- and micro-aggregates in triplicate, carefully placed them on a glass fiber filter paper, and allowed them to gently humidify over a 24-hour period (Lehmann, Kinyangi, and Solomon 2007). Subsequently, the undisturbed soil aggregates underwent freezing at  $-20^{\circ}\text{C}$  and were cryo-ultramicrotomed to  $1\ \mu\text{m}$  thickness using a stainless-steel knife in a cryomicrotome (Cryotome E, Thermo Shandon Limited, UK). The resulting thin sections were then placed onto MirrIR Low-E microscope slides (Kevley Technologies, Ohio, USA) for further analysis.

The samples underwent triplicate analysis at beamlines 01B and 06B of the Shanghai Synchrotron Radiation Facility (SSRF). This generated a total of 303 individual spectra for Barrow soils, 419 spectra for Creamers Field soils, and 729 spectra for Jago soils. Spectral maps were acquired in reflection mode across a scanning wavenumber range from  $650$  to  $4000\text{cm}^{-1}$ . Parameters included an aperture size of  $10 \times 10\ \mu\text{m}^2$ , a step size of  $10 \times 10\ \mu\text{m}^2$ , a resolution of  $4\text{cm}^{-1}$ , and 64 co-added scans. Subsequent processing of the spectral maps was carried out using OMNIC 9.0 (Thermo Fisher Scientific Inc., Waltham, USA). This allowed for accurate depiction of characteristic peak intensities and spatial distribution positions of each functional group. The specific IR absorbances subjected to analysis were as follows:  $3621\text{cm}^{-1}$  (mineral-OH),  $2922\text{cm}^{-1}$  (lipids),  $1634\text{cm}^{-1}$  (amides),  $1525\text{cm}^{-1}$  (lignin), and  $1080\text{cm}^{-1}$  (polysaccharides) (Lehmann, Kinyangi, and Solomon 2007; Shabtai et al. 2023; Sun et al. 2023; Wasner et al. 2024; Weng et al. 2022). Among these functional groups, amides ( $1634\text{cm}^{-1}$ ) are attributed to microbial-derived biopolymers, whereas lipids ( $2922\text{cm}^{-1}$ ),  $1525\text{cm}^{-1}$  (lignin), and polysaccharides ( $1080\text{cm}^{-1}$ ) may mainly originate from plant-derived products (Kang et al. 2024; Wasner et al. 2024). We acknowledge that the peak at  $1080\text{cm}^{-1}$ , referred here as polysaccharides, also encompasses peaks originating from Si-O vibrations associated with clay minerals. Utilizing the absorption peak intensities of each functional group, a false-color 2D map was generated for image processing purposes. These intensities, in conjunction with linear regression, were used to assess the spatial correlation between mineral-OH and selected C functional groups (Xu et al. 2024). The detailed dataset is available in Data S4.

Following the synchrotron radiation-based IR spectromicroscopy analysis, chemical images of iron (Fe) were acquired at beamline 15U1 of the SSRF, covering the identical regions as the thin sections. Fluorescence maps depicting Fe were created by scanning the samples using a monochromatic beam at  $E = 10\text{keV}$ , using a step size of  $6 \times 8\ \mu\text{m}^2$ , and a dwell time of 5 s (Yu et al. 2021).

## 2.6 | Cultivation Experiment

To investigate the impact of varying moisture contents on the peroxidase activity of soils, a cultivation experiment

was conducted (Figure S2). Three grams of each sample was weighed and placed into 50-mL flasks. These samples were then adjusted with ultrapure water to five different volumetric moisture content levels (0%, 20%, 40%, 60%, 80%). The flasks were carefully sealed with a film to minimize water evaporation while still allowing for gas exchange. The soils were subjected to aerobic cultivation at  $10^{\circ}\text{C}$  in darkness for a duration of 2 days (with a total of  $n = 120$  samples, 12 replicates per soil samples). The moisture levels were monitored gravimetrically, and any lost moisture was replenished daily by adding ultrapure water. Following this cultivation period, the soils were thoroughly mixed and promptly analyzed to determine their peroxidase activity.

## 2.7 | Biogeochemical Analyses

SOC and nitrogen (N) contents in soils were measured using an elemental analyzer (Elementar EL cube, Elementar, Hanau, Germany) after eliminating carbonates with 1 M HCl. The  $\delta^{13}\text{C}$  and  $\delta^{15}\text{N}$  composition were determined based on soil C and N content using an elemental analyzer-isotopic ratio mass spectrometer (253 Plus, Thermo Scientific, Waltham, USA). For radiocarbon analysis, dried soils, following carbonate removal, underwent combustion in tin boats and were transformed into elemental C through an automated graphitization system (AGE) (Altenburg, Machts, and Steinhof 2017). Radiocarbon analyses were performed using the 0.5 MV Tandemron Accelerator Mass Spectrometer (AMS; NECL.5SDH-1, USA) in the School of Earth System Science, Tianjin University. Results include conventional radiocarbon ( $\Delta^{14}\text{C}$ ) ages (BP) and  $\Delta^{14}\text{C}$  values (in ‰), both corrected for exogenous C contributions and isotopic fractionation, along with a 1-sigma measurement uncertainty (Altenburg, Machts, and Steinhof 2017). Soil  $\text{H}_2\text{O}_2$  levels were determined using the titanium sulfate colorimetric method at 415 nm (Satterfield and Bonnell 1955), employing a hydrogen peroxide content detection kit from Beijing Solarbio Science & Technology Co., Ltd. This analysis was conducted on a SpectraMax M5 spectrophotometer (Molecular Devices, Sunnyvale, CA).

Short range-ordered (SRO) minerals were obtained using the acid ammonium oxalate method (Blakemore, Searle, and Daly 1981). The calculation involved determining  $\text{Al}_0 + 1/2\text{Fe}_0$ , where  $\text{Fe}_0$  and  $\text{Al}_0$  represent the Fe and Al content that was quantified using inductively coupled plasma optical emission spectrometer (ICP-OES) (5110, Agilent, Melbourne, Australia). Reactive iron minerals ( $\text{Fe}_{\text{DCB}}$ ) and Fe-bound organic carbon (Fe-bound OC) were evaluated using the adapted dithionite-citrate-bicarbonate (DCB) method (Lalonde et al. 2012; Mehra and Jackson 1958), employing a 0.1 M DCB solution. Briefly, 0.25 g of finely ground soils were introduced into a solution containing a buffer (sodium bicarbonate, pH 7.3) and a metal ion complexing agent (0.68 M sodium citrate) in sealed 50-mL Teflon tubes, and the mixture was heated to  $80^{\circ}\text{C}$  in a water bath. A reducing agent (0.4 g of sodium dithionite) was added, and the solution was maintained at  $80^{\circ}\text{C}$  for 15 min. The reduction reaction took place at an almost neutral pH, with sodium bicarbonate acting as a buffer to prevent organic matter hydrolysis, protonation, and re-adsorption onto soils, which could occur under acidic conditions. Control experiments

were conducted concurrently, wherein samples were extracted under the same conditions as the reduction treatment, but sodium citrate and sodium dithionite were replaced with NaCl, to assess the extent of OC desorption from the soils. The resulting suspensions were filtered through 0.45- $\mu\text{m}$  filters and dissolved iron concentration ( $\text{Fe}_{\text{DCB}}$ ) was quantified using ICP-OES (5110, Agilent, Melbourne, Australia). The percentage of Fe-bound organic carbon (Fe-bound OC) was calculated using Equation (6):

$$\text{Fe-bound OC (\%)} = (\text{OC}_{\text{NaCl}} - \text{OC}_{\text{DCB}}) / \text{SOC} \times 100, \quad (6)$$

where  $\text{OC}_{\text{NaCl}}$  and  $\text{OC}_{\text{DCB}}$  represent the OC content of the NaCl- and DCB-treated soil residues, respectively. Both  $\text{OC}_{\text{NaCl}}$  and  $\text{OC}_{\text{DCB}}$  were quantified using a total organic carbon/total nitrogen analyzer (OI Analytical 1030 W + 1088, USA).

## 2.8 | Statistical Analyses

Statistical analyses were conducted using SPSS 19.0 (SPSS, Chicago, IL). To assess differences between the upper and deep layers of permafrost samples, one-way analysis of variance (ANOVA) coupled with Tukey's honest significance test (HSD) was conducted, assuming normality and homogeneity of variance conditions. Different letters (means  $\pm$  SD,  $n=3$ ) represent significant differences among treatments at a significance level of  $p < 0.05$ . A structural equation modeling (SEM) was constructed by using the AMOS software to analyze the relationships between potential mineralogical and biomarker predictors on soil C persistence. Variation partitioning analysis (Legendre 2007) was further performed to quantify the separate influence of hydrogen peroxide and SRO minerals on peroxidase activity. Geographical information system (GIS) tools within GPS were utilized to present an overview of the study area. The mapping data underwent further processing and analysis using Origin 9.0 software. The coefficient of determination ( $R^2$ ) was utilized to assess the relationship between two variables. For the identification and processing of data obtained through synchrotron radiation-based IR spectromicroscopy, OMNIC 9 (Thermo Nicolet, Madison, USA) and Analysis Studio 3.15 (Anasys Instrument Inc., Santa Barbara, USA) were used, respectively.

## 3 | Results

### 3.1 | Soil Microbial Necromass Carbon and Soil Carbon Ages

All eight examined permafrost soils exhibited millennial-scale radiocarbon ( $\Delta^{14}\text{C}$ ) ages, spanning from 3.1 to 14.7 thousand years before present (kyr BP) (Figure 1b and Table 1). As expected, deeper subsoils ( $> 140\text{ cm}$ ) were considerably older than upper subsoils ( $< 70\text{ cm}$ ) across the permafrost soil profile (Figure 2a). A strong correlation between soil C age (derived from radiocarbon composition) and depth (Figure 2a) indicated that soil C persistence increased with depth. A coupled isotopic  $\Delta^{14}\text{C}$  and  $\delta^{13}\text{C}$  plot (Figure S3) revealed a negative correlation, suggesting that older C exhibited a higher enrichment in  $^{13}\text{C}$ .

Both bacterial and fungal necromass C exhibited strong correlations with SOC, yet they comprised only a minor portion of SOC in Alaskan permafrost soils, accounting for 3% and 9%, respectively (Figure 2b,c). SOC displayed a threefold higher linear coefficient with fungal necromass C compared to bacterial necromass C (Figure 2b,c), consistent with the high fungal/bacterial necromass ratios (Table S5). However, when quantifying the contribution of microbial necromass to SOC accumulation, the microbial necromass C contributed only  $\sim 10\%$ – $15\%$  to SOC in Alaskan permafrost soils (Figure 2d), while the percentage in soils from the global survey is  $\sim 30\%$ – $60\%$  (representing the 25th–75th population percentiles) (Figure 2d). This average contribution of microbial necromass C in Alaskan permafrost soils could potentially rise to  $\sim 11\%$ – $19\%$  (Figure S4 and Table S4) according to updated equations (Equations 3 and 4). Moreover, earlier estimates may have overrated the contribution of bacterial necromass while underrating that of fungal necromass (Figure S4 and Table S4). Further, our plot of  $\delta^{13}\text{C}$  and C/N ratios suggest the predominance of plant residues in Alaskan permafrost soils (Figure S5). This predominance is partly due to terrestrial plants using the C3 photosynthetic pathway, which typically yields  $\delta^{13}\text{C}$  values between  $-32\%$  and  $-21\%$  and relatively high C/N ratios exceeding 12.

### 3.2 | Mineralogical Control on Soil Carbon Abundance

A positive correlation between the ratio of reactive Fe to total Fe ( $\text{Fe}_{\text{DCB}}/\text{Fe}_t$ ) and soil C abundance was observed, including SOC, bacterial and fungal necromass C (Figure 3 and Table S2). However, there was no discernible correlation between soil C abundance and single mineral index ( $\text{Fe}_{\text{DCB}}$ , SRO, and water-extracted Fe). This observation was corroborated by Fourier transform infrared (FTIR) results (Figure 3). In contrast, plant- and microbial-derived biopolymers derived from FTIR, including lipids ( $2922\text{ cm}^{-1}$ ) and amides ( $1634\text{ cm}^{-1}$ ), exhibited a positive correlation with  $\text{Fe}_{\text{DCB}}/\text{Fe}_t$ . FTIR spectra also revealed a positive correlation of organic functional groups with the structural hydroxyl (OH) groups in minerals ( $3620\text{ cm}^{-1}$ ) (Figure S6). In summary, reactive minerals such as  $\text{Fe}_{\text{DCB}}$  and SRO exhibited no correlation with microbial necromass C and SOC. Conversely, the degree of mineral weathering (indicative by  $\text{Fe}_{\text{DCB}}/\text{Fe}_t$ ) may play a crucial role in the preservation of microbial necromass C and SOC.

### 3.3 | Correlation Between Peroxidase Activity and Soil Carbon Persistence

Peroxidase activity involves the conversion of  $\text{H}_2\text{O}_2$  into water, which triggers the oxidation process of colorless 3,3',5,5'-tetramethylbenzidine (TMB) to its blue oxidized form (oxTMB, Figure 4a). Similar to natural horseradish peroxidase (Figure S8), permafrost soils with varying iron mineral composition (Figure S9) exhibited the ability to catalyze the conversion of colorless TMB into blue oxTMB in the presence of  $\text{H}_2\text{O}_2$  (Figure 4b and Data S3). Through a comparison of the peroxidase activity between the extracted soil solution and the gathered soil particles under identical conditions (Figure S8), we found that the peroxidase activity was indeed retained in the

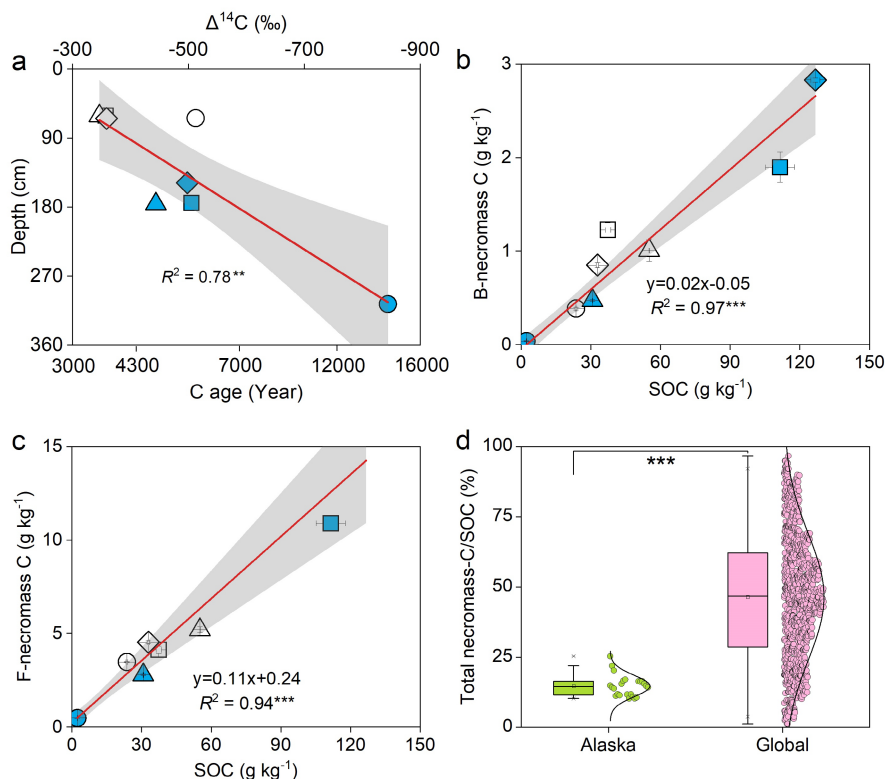


**FIGURE 2** | Soil  $\Delta^{14}\text{C}$  and the percentage of total necromass C in SOC. (a) Development of soil  $\Delta^{14}\text{C}$  and C ages with depth. Soil cores 1–4 are marked by square, circle, triangle, and diamond symbols, respectively. Hollow and solid shapes differentiate between the upper and deep layers, respectively. (b) Correlation between SOC and bacterial (B)-necromass C. (c) Correlation between SOC and fungal (F)-necromass C. Regression lines ( $p < 0.05$ ) are depicted, with shaded areas representing 95% confidence intervals. (d) Boxplots comparing total necromass-C/SOC ratios among Alaska (from this study) and global soils based on existing literature (Data S2). SOC, soil organic carbon. Data in (b) and (c) are presented as mean and SE ( $n = 3$ ). The boxes in (d) represent the interquartile range (IQR) divided by the median, while the whiskers extend 1.5 times IQR. The dataset for (d) includes  $n = 24$  (8 soils in triplicates from three different locations) for Alaska from this study and 1200 for global soils. Two-tailed unpaired  $t$  tests determined the  $p$  values. \*\* $p < 0.01$ , \*\*\* $p < 0.001$ .

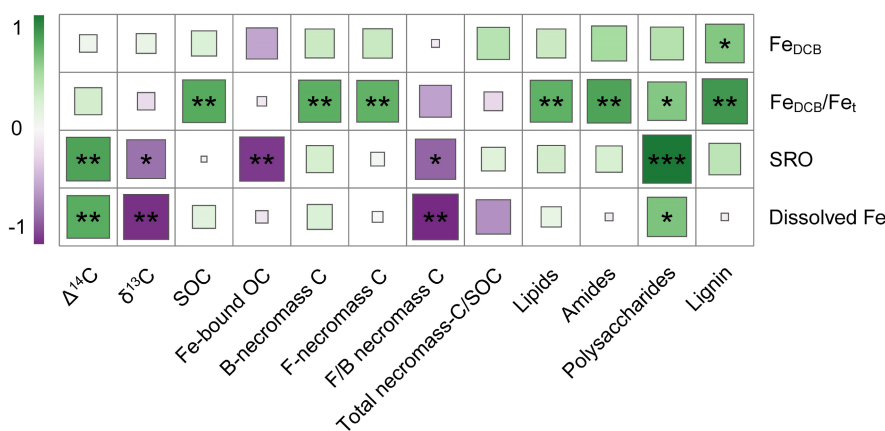


**FIGURE 3** | Heatmap depicting correlations between mineral variables and soil C properties.  $\Delta^{14}\text{C}$  and  $\delta^{13}\text{C}$  represent carbon age and the degree of microbial utilization, respectively. B-necromass, bacterial necromass; F-necromass, fungal necromass. Total necromass combines B-necromass and F-necromass. SOC, soil organic carbon. Lipids, amides and polysaccharides are differentiated by their infrared peak heights at 2922, 1634, and 1080  $\text{cm}^{-1}$ , respectively.  $\text{Fe}_{\text{DCB}}$  and Fe-bound OC denote the reactive iron oxide and the portion of organic carbon (OC) associated with reactive minerals, extracted using the dithionite-citrate-bicarbonate (DCB) method (Mehra and Jackson 1958). SRO stands for short-range-ordered (SRO) minerals extracted via the acid oxalate method (Blakemore, Searle, and Daly 1981).  $\text{Fe}_t$  (total Fe) is determined using X-ray fluorescence spectrometry.  $\text{Fe}_{\text{DCB}}/\text{Fe}_t$  denotes the degree of mineral weathering (Doetterl et al. 2018). Water-extracted Fe is quantified using ICP-OES after shaking extraction with water (soil-water ratio 1:5). Darker shades and higher absolute values in the squares indicate a strong correlation between the explanatory and response variables. Significance is indicated as follows: \* $p < 0.05$ , \*\* $p < 0.01$ , \*\*\* $p < 0.001$ .  $n = 24$  (eight soils in triplicates from three different locations).

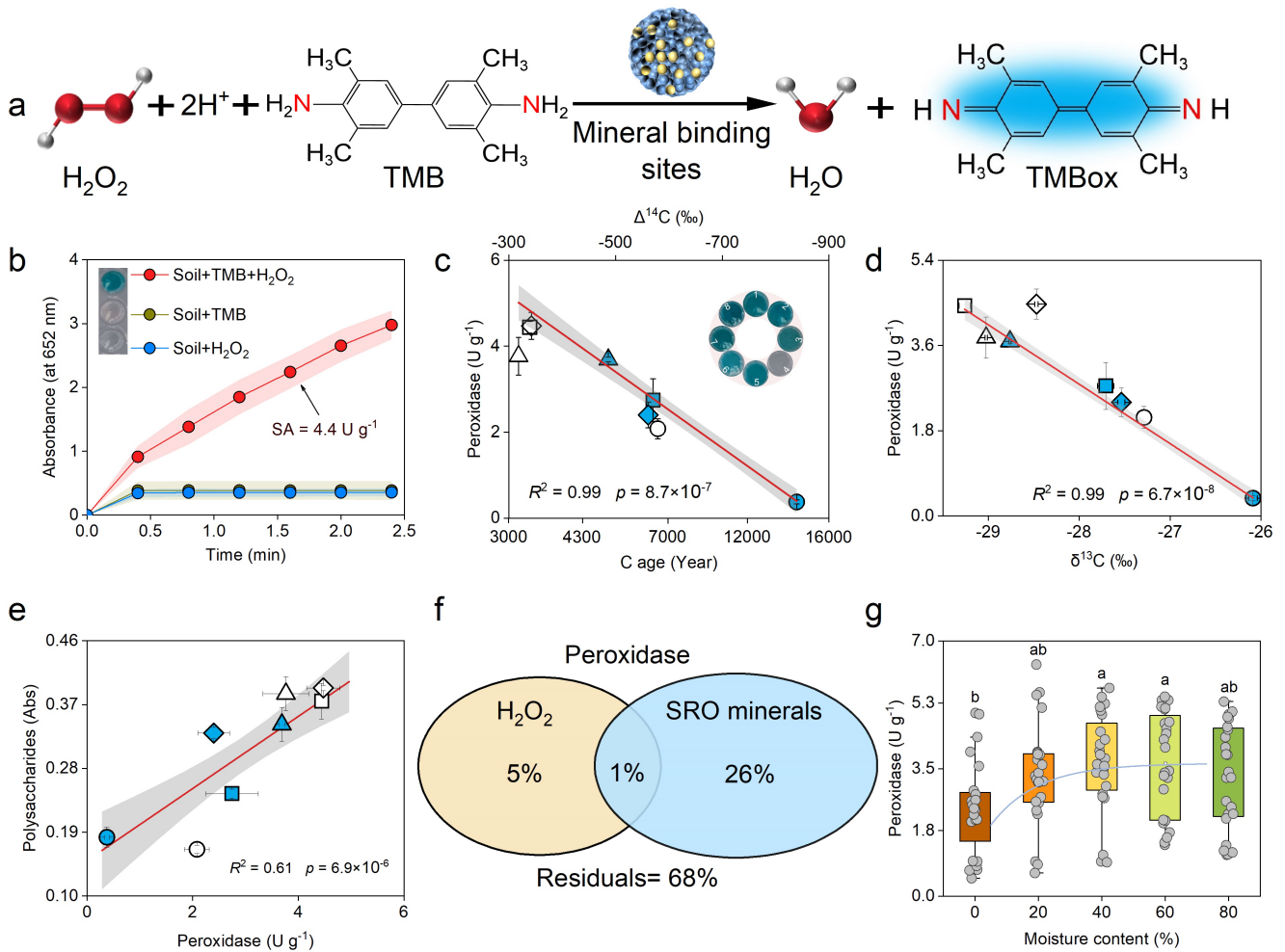


**FIGURE 4** | Peroxidase activity controlling soil carbon persistence. (a) Schematic illustration of the assessment principle for peroxidase activity in permafrost soils. Peroxidases, denoting mineral active sites (Zandieh and Liu 2021), catalyze the conversion of colorless 3,3',5,5'-tetramethylbenzidine (TMB) into its blue oxidized form (oxTMB) in the presence of  $H_2O_2$  (Jiang et al. 2018). (b) Typical curves depicting soil-catalyzed TMB colorimetric reaction obtained for the permafrost soil (Barrow at 57–64 cm). (c) Correlation between peroxidase activity and C ages, as well as  $\Delta^{14}C$ . (d) Correlation between peroxidase activity and  $\delta^{13}C$ . Numbers in the schematic diagram of color development correspond to samples in Figure 2. Lines in (c, d) indicate significant regressions ( $p < 0.05$ ), and shaded areas represent 95% confidence intervals. (e) Correlation between peroxidase activity and polysaccharide absorbance (as characterized by FTIR). (f) Variation partitioning analysis for peroxidase activity suggests that their interactive effects between amorphous minerals and  $H_2O_2$  exert only 32% influence on peroxidase activity. (g) Changes in peroxidase activity with volumetric soil moisture contents. Distinct letters in (g) indicate significant differences between moisture content groups, determined using one-way ANOVA followed by Tukey's HSD post hoc tests at  $p < 0.05$ , adhering to conditions of normality and homogeneity of variance.  $n = 24$  in (g).

collected soil particles, suggesting that a strong adsorption of extracellular peroxidases on minerals or the minerals themselves contribute to this peroxidase activity.

The peroxidase activity displayed a high correlation coefficient ( $R^2 = 0.99$ ,  $p < 10^{-6}$ ) with  $\Delta^{14}C$  and  $\delta^{13}C$  (Figure 4c,d). This strong correlation indicates a dominant control for peroxidase on soil C persistence, suggesting that “older” C may persist through eliminating peroxidase activity in permafrost soils. A positive correlation between peroxidase and polysaccharides (Figure 5e) reflected that reduced peroxidase activity may result in the degradation of plant residues in permafrost soils. Structure equation modelling (SEM) analysis further revealed that peroxidase activity exerted the predominant control on soil C persistence, likely facilitated by the contribution of amorphous or SRO minerals (Figure S10). To address

the individual and combined effects of edaphic and microbial factors on peroxidase activity, variation partitioning analysis (VPA) was conducted. VPA indicated that  $H_2O_2$  and SRO minerals collectively accounted for 32% of the variability in peroxidase activity, but mineral characteristics exert a greater influence (26% vs. 5%) on peroxidase activity compared to  $H_2O_2$  levels (Figure 4f, Figures S11 and S12). A significant portion, up to 68%, remained unexplained.

The stability of soil C in permafrost ecosystems is potentially influenced by changes in moisture levels, such as freeze–thaw cycles and precipitation patterns. To investigate whether moisture availability could affect peroxidase activity and potentially destabilize soil C, a cultivation experiment involving permafrost soils exposed to varying moisture levels (0%–80% by volume) was conducted (Figure 4g and Figure S2). A substantial increase

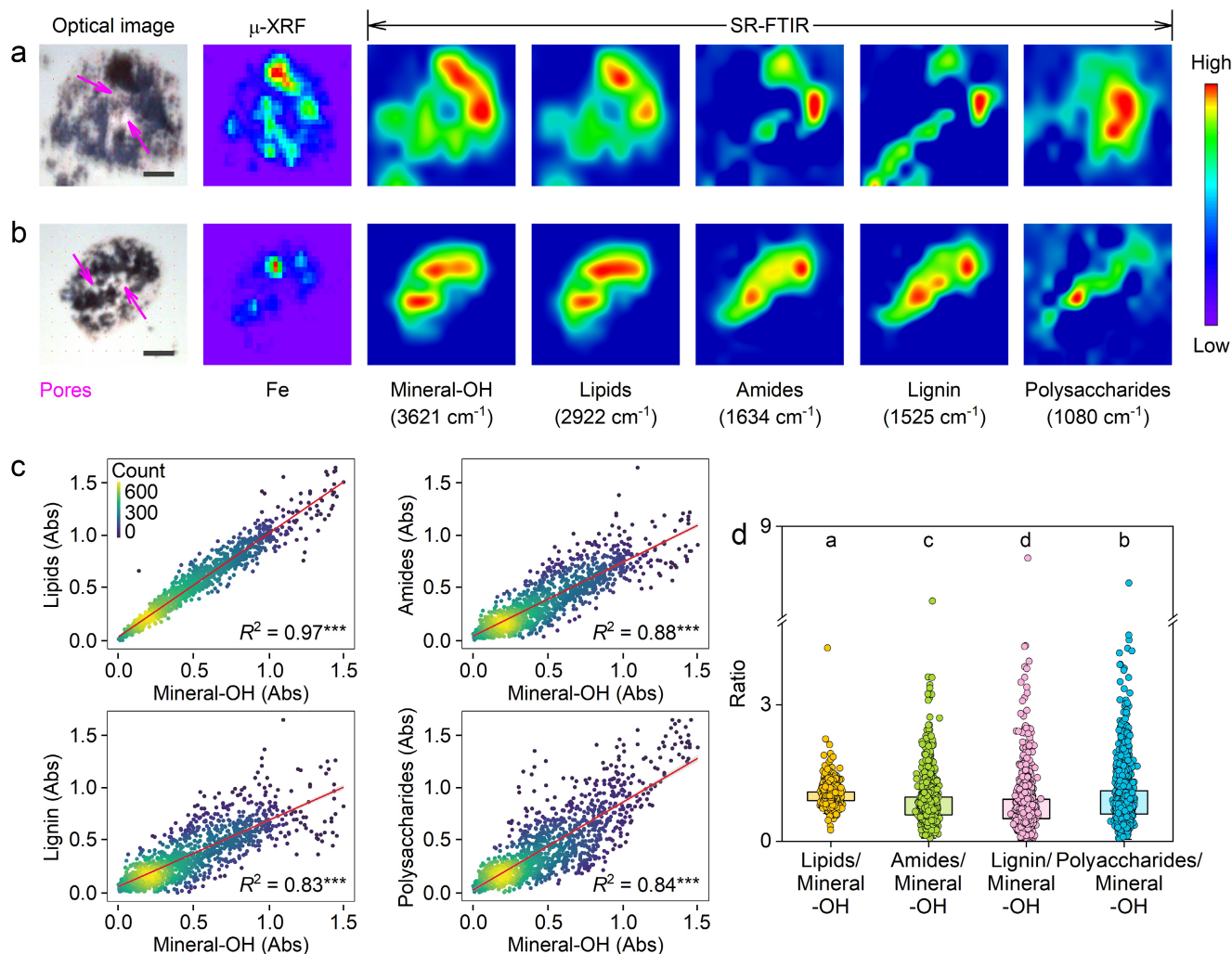


**FIGURE 5** | Microscale analysis of minerals' control on microbial- and plant-derived biopolymers in soil aggregates, elucidated through correlative synchrotron radiation infrared (IR) and  $\mu$ -XRF spectromicroscopy. (a and b) Typical soil aggregates. Purple arrows indicate soil pores. Scale bar is 20  $\mu\text{m}$ . (c) Correlation between mineral-OH (O–H, 3621  $\text{cm}^{-1}$ ) and microbial- and plant-derived biopolymers. (d) Changes in ratios between microbial- and plant-derived biopolymers and minerals suggesting the distinct retention of microbial- and plant-derived biopolymers by mineral surfaces. The organic functional groups selected for analysis include lipids (C–H, 2922  $\text{cm}^{-1}$ ), amides (N–H, 1634  $\text{cm}^{-1}$ ), lignin (C=C, 1525  $\text{cm}^{-1}$ ), and polysaccharides (C–OH, 1080  $\text{cm}^{-1}$ ) (Data S4). The correlation analyses encompass  $n = 1451$  data points collected from 24 soils (8 soils in triplicates from 3 different locations).  $^{***}p < 0.001$ . Distinct letters in (d) indicate significant differences between moisture content groups, determined using one-way ANOVA followed by Tukey's HSD post hoc tests at  $p < 0.05$ , adhering to conditions of normality and homogeneity of variance.  $\mu$ -XRF, micro-X-ray fluorescence spectromicroscopy.

( $p < 0.01$ ) in soil peroxidase activity in the range of 0%–40% was observed as moisture content increased. Peroxidase activity remained relatively stable ( $p > 0.05$ ) in soils with moisture contents between 40% and 60% but slightly decreased in the range of 60% to 80%.

### 3.4 | In Situ Observation of Mineral Retention on Plant- and Microbial-Derived Biopolymers

The  $\mu$ -XRF mapping revealed the presence of nanoscale to submicron scale Fe (oxyhydr)oxides in soil aggregates, suggesting that the structure OH groups (3621  $\text{cm}^{-1}$ ) in minerals may partly originate from Fe (oxyhydr)oxides, particularly goethite (Figure 5 and Figure S9). By examining 1451 individual spectra extracted from the entire sample set, strong correlations between

mineral-OH and biopolymers were found ( $R^2 = 0.83$ – $0.97$ ), including lipids (C–H, 2922  $\text{cm}^{-1}$ ), amides (N–H, 1634  $\text{cm}^{-1}$ ), lignin (C=C, 1525  $\text{cm}^{-1}$ ), and polysaccharides (C–OH, 1080  $\text{cm}^{-1}$ ) (Figure 5, Figures S14 and S15). Remarkably, the average ratio of lipids with mineral-OH was the highest, followed by that of polysaccharides, amides, and lignin.

## 4 | Discussion

### 4.1 | Contribution of Microbial Residues to Permafrost Carbon Cycling

Compared to other ecosystems, higher latitude Alaskan permafrost contains elevated levels of C and microbial biomass in deep soils (Crowther et al. 2019). Although these deep

soils harbor a large SOC pool, only one study, to the best of our knowledge, has measured microbial necromass in Arctic permafrost soils (Dai et al. 2002). We show that Alaskan permafrost subsoils contain less than 15% microbial necromass C, which was 2 to 6 times lower than the global average (Figure 2). This finding is bolstered by the new equations proposed by Hu et al. (2024). The estimated contributions of microbial necromass C to SOC from both references showed a strong correlation and were quite similar (Figure S4 and Table S4). In Alaskan permafrost soils, the average contribution of microbial necromass C could potentially rise to ~11%–19% (Figure S4 and Table S4) according to updated equations (Equations 3 and 4). Previous estimates may have overrated bacterial necromass contributions while underrating fungal contributions (Figure S4 and Table S4). By integrating machine learning approaches with the proportional contribution of bacterial groups, the new equations proposed by Hu et al. (2024) decreased the contribution of bacterial residues to microbial necromass. Our findings suggest that the ratios of fungal to bacterial necromass C were underestimated by ~43% (Figure S4 and Table S4), highlighting the critical yet underestimated role of fungi processes in soil C cycles in permafrost regions. This substantiates previous conjectures that microbial necromass contributes to a minor extent to permafrost SOC (Dai et al. 2002; Hu et al. 2024), which is predominantly derived from plant residues (García-Palacios et al. 2024).

While the current favored method relies on amino sugars for quantifying microbial necromass C (Hu et al. 2024; Liang et al. 2019), it may overlook microbial extracellular biopolymers that could be recycled or stabilized in soils. This study introduces a complementary platform, combining gas chromatography (GC) with synchrotron-based IR spectromicroscopy, for assessing both microbial necromass and extracellular biopolymers in soils, respectively. It is acknowledged that necromass persistence is documented not only by amino sugars but also by proteins and extracellular polysaccharides (Buckeridge, Creamer, and Whitaker 2022; Hall et al. 2020). Nearly all soil microbial life, estimated at around  $3 \times 10^{29}$  cells of bacteria and archaea, is thought to reside in biofilms made up of cells and extracellular polymeric substances (Flemming and Wuertz 2019). While living microbial biomass constitutes less than 5% of SOC, microbial necromass accounts for over 50% (Hu et al. 2024; Figure 2d), indicating that extracellular biopolymers and amino sugars persist over time after individual cell death in soils. However, directly characterizing extracellular products in soil is challenging due to the complexity of the soil matrix (Camenzind et al. 2023). Notably, this study demonstrates that synchrotron radiation-based IR spectromicroscopy can identify spatial connections between key microbial components (e.g., proteins) and structural hydroxyl groups in minerals at submicron scales (Figure 5, Figures S13 and S14). This technique offers valuable insights into the in situ preservation of extracellular biopolymer by minerals. Additionally, the spatial correlation between hydroxyl functional groups on mineral surfaces and specific C functional groups points to a selective protection mechanism for minerals during the burial of extracellular C at the level of functional groups (Chang, Yu, and Liu 2023; Xu et al. 2024). Given that ligand exchange between C functional groups in SOM and hydroxyl groups in minerals is a primary mechanism for C preservation (Gu et al. 1994; Kaiser et al. 1997), using synchrotron radiation-based IR spectromicroscopy is

essential for investigating the mechanisms behind soil C stability and persistence, owing to its ability to simultaneously detect spatially related C and hydroxyl groups in minerals.

Beyond its role in detecting mineral protection, this technique can also explore various other stabilization processes, including organo-organic interactions (Buckeridge et al. 2020; Possinger et al. 2020). These interactions, where extracellular biopolymers adhere to other forms of necromass or plant residues (such as polysaccharides) (Kang et al. 2024), are often overlooked yet play a crucial role (Vogel et al. 2014). Furthermore, by analyzing the ratios of aliphatic, aromatic, and phenolic components alongside polysaccharides (like peaks at 2920/1030, 1630/1030, 1515/1030<sup>-1</sup>) to derive humification indices (Broder et al. 2012; Hodgkins et al. 2014), this technique demonstrates potential for visually assessing the degree of decomposition of extracellular biopolymers within soil aggregates. Overall, integrating chemolytic biomarker analysis with synchrotron-based IR spectromicroscopy enhances our understanding of the stabilization of both amino acids and extracellular biopolymers in soils, which is crucial for conceptualizing their role within the broader framework of biogeochemical cycles and C storage dynamics.

## 4.2 | Factors and Mechanisms Affecting the Accrual and Stabilization of Permafrost Soil Carbon

Given the minor proportion of microbial necromass and its weak connection with reactive minerals (Figures 1 and 2), it is reasonable that the necromass stabilization mechanism in Alaskan permafrost soils is less significant than in Tibetan (He et al. 2022) or temperate regions (Kang et al. 2024; Liang et al. 2019; Wang et al. 2021). This inference is supported by the higher average ratio of lipids, deriving from plant sources (Wasner et al. 2024), with mineral-OH than amides, representing microbial sources (Figure 5c), providing evidence to refute the preference absorbance of microbial residues on minerals in Alaskan permafrost subsoils.

Our findings indicate that peroxidase activity has a strong predictive capability for soil C persistence, supporting the “peroxidase-driven carbon stabilization hypothesis”, which suggests that long-term carbon accumulation may rely on maintaining low levels of peroxidase activity. The coefficient between peroxidase and C age (Figure 4c,d) exceeded that of SRO minerals with SOC ( $p < 10^{-2}$ ) by four orders of magnitude (Figure 3). In addition to peroxidase activity, this colorimetric approach also denotes mineral active sites in samples (Robert and Meunier 2022; Zandieh and Liu 2021; Zhang et al. 2021), which is consistent with a strong connection between structural OH in minerals and C functional groups at the submicron scale (Figure 5c).

Peroxidase activity may stem from mineral-bound extracellular enzymes (Allison 2006; Jones et al. 2020) and minerals themselves (Safarik and Prochazkova 2022, 2024). Mineral stabilization of peroxidases has been shown to preserve high oxidative potential in soils during dry periods, leading to rapid OM degradation during wet periods (Darrouzet-Nardi et al. 2023; Stursova and Sinsabaugh 2008). Recent studies have demonstrated that magnetically responsive minerals isolated from soils (Safarik and Prochazkova 2022), as well as montmorillonite (Safarik and

Prochazkova 2024) exhibit notable peroxidase mimetic activity. This reveals the complexity of mineral-SOC interactions, especially in unique soils like Arctic permafrost soils, which allow the presence of a substantial amount of  $H_2O_2$  (Page et al. 2013; Trusiak et al. 2018). Compared to indicators of extractable minerals (such as SRO or water-extracted Fe) (Figure 3), the notably higher significance of peroxidase activity in predicting soil C persistence (Figure 4) may be attributed to the fact that only a fraction of SOC is influenced by poorly crystalline or water-extracted ions (Jaworska, Dąbkowska-Naskręć, and Kobierski 2016), while non-extractable minerals or mineral-bound extracellular enzymes may play more essential roles (Coward, Thompson, and Plante 2017).

This is supported by a better correlation between  $Fe_{DCB}/Fe_t$  and C components than single mineral index ( $Fe_{DCB}$ , SRO, and water-extracted Fe) (Figures 3 and 4). As  $Fe_{DCB}/Fe_t$  is indicative of mineral weathering degree (Doetterl et al. 2018), our findings suggest that increased soil weathering, rather than solely the content of reactive minerals stabilizes SOC and contributes to its persistence in permafrost soils. microbial necromass.

### 4.3 | Implications for the Vulnerability of Permafrost Soils in Facing Climate Changes

Soil peroxidase activity plays a crucial role in the long-term stabilization of SOC and microbially derived C by mediating essential ecosystem functions, including lignin degradation, SOC mineralization, and dissolved SOC export (Sinsabaugh et al. 2008; Sinsabaugh 2010; Tian and Shi 2014). For example, peroxidase activity accounts for ~30% of SOC contents across various ecosystems (Sinsabaugh 2010). In our study, we manipulated volumetric moisture content in subsoils from Alaskan permafrost, which affects peroxidase activity that likely has an impact on the persistent SOC (Figure 4). High peroxidase activity tends to limit SOC accumulation, while low activity promotes SOC storage (Sinsabaugh et al. 2008). This highlights how close changes in oxidative enzyme activities due to changing soil environment is linked to SOC sensitivity, which could significantly influence global C cycling. While the importance of soil peroxidase activity in SOC stabilization has been noted (Sinsabaugh et al. 2008; Sinsabaugh 2010; Tian and Shi 2014), prior research mainly focused on surface soils. Our study is the first to examine the effects of peroxidase activity on deep permafrost soils. Given the substantial SOC reservoir and low necromass composition in Alaskan permafrost, these findings are vital for understanding the vulnerability of deep permafrost soils amid climate change-induced thawing (Schuur et al. 2022).

Similarly, at the ecosystem scale, peroxidase activities in surface soils were shown to correlate with mass loss rate in particulate OM and with changes in SOM content (Sinsabaugh 2010; Sinsabaugh et al. 2008). This susceptibility likely stems from the catalytic effects of both mineral-bound extracellular enzymes and mineral-derived ROS on SOC, suggesting that ancient C previously locked by freezing in these ecosystems may be prone to destabilization in the face of climate change. The destabilized old C is not replenished over a short period, potentially representing a new source of  $CO_2$  to the atmosphere, potentially diminishing the size of the SOC reservoir in an irreversible manner.

Considering the widespread presence of  $H_2O_2$  in permafrost soils (Page et al. 2013; Trusiak et al. 2018), our findings highlight the intricate nature of mineral mediated-soil C cycles in permafrost ecosystems. Understanding the mechanistic drivers of C persistence is crucial for predicting its susceptibility to global change (Heckman et al. 2022). For instance, during increases in moisture availability (e.g., permafrost thaw), conditions like water-logging and limited oxygen can lead to reducing conditions, resulting in the formation of Fe(II) (Patzner et al. 2020; Patzner, Kainz, et al. 2022; Patzner, Logan, et al. 2022). Given changes in wetting or drying post-permafrost thaw (Ping et al. 2015), coupled with the potential for increased intensity of rainfall events in the northern permafrost region (Teufel and Sushama 2019), permafrost thaw and increased precipitation may initiate a series of positive feedbacks that increase the vulnerability of persistent C and trigger a robust permafrost C-climate feedback loop.

## 5 | Conclusions

We provide evidence from biomarkers that Alaskan permafrost subsoils contain less than 15% microbial necromass carbon, which is significantly below the global average. Notably, peroxidase activity is a strong predictor of soil carbon persistence in Alaskan permafrost, and long-term carbon accumulation may depend on sustaining low peroxidase activity levels. However, enhancement in moisture availability, particularly within the 0%–40% moisture content range, can increase peroxidase activity in soils. This finding suggests that ancient carbon in Alaskan permafrost may be vulnerable to moisture-driven destabilization with high moisture contents. Thus, moisture availability may represent a critical trigger for releasing persistent carbon by changing soil peroxidase. Collectively, our findings advance the understanding of the mechanisms governing soil carbon persistence in Arctic permafrost soils, enabling us to better predict its response to global changes.

We also showed that synchrotron radiation-based infrared spectromicroscopy can identify spatial connections between key microbial biopolymers (e.g., proteins) and structural hydroxyl groups in minerals. This technique complements chemolytic biomarker analysis by recognizing that necromass persistence is documented not only in amino sugars but also in excretions like proteins and extracellular polysaccharides. Thus, integrating chemolytic biomarker analysis with synchrotron-based IR spectromicroscopy improves our understanding of how amino acids and extracellular biopolymers stabilize in soils, which is vital for grasping their role in biogeochemical cycles and carbon storage dynamics. Since some extraction methods, such as acid ammonium oxalate and dithionite-citrate-bicarbonate methods, may lack selectivity or quantitative accuracy, this study advocates a shift towards colorimetric or spectroscopic approaches to evaluate organo-mineral interactions in soils.

### Author Contributions

**Yi-Xuan Guo:** data curation, formal analysis, methodology, software, visualization, writing – original draft, writing – review and editing. **Guang-Hui Yu:** conceptualization, formal analysis, funding acquisition, investigation, resources, supervision, writing – original draft, writing – review and editing. **Shuijin Hu:** writing – review and editing. **Chao Liang:** methodology, writing – review and editing. **Andreas Kappler:**

writing – review and editing. **Mark Torre Jorgenson**: resources, writing – review and editing. **Laodong Guo**: resources, writing – review and editing. **Georg Guggenberger**: writing – review and editing.

## Acknowledgements

The authors thank the technical support at the BL01B1, BL06B1, BL11B, BL14W, and BL15U beamlines at the Shanghai Synchrotron Radiation Facility (SSRF). This work was supported by the National Natural Science Foundation of China (U22A20608, 32241037, and 41977271) and Tianjin Municipal Science and Technology Bureau (23ZYJDC00050, 24ZYJDC00330).

## Conflicts of Interest

The authors declare no conflicts of interest.

## Data Availability Statement

The data that support the findings of this study are openly available in Zenodo at <https://doi.org/10.6084/m9.figshare.25249345> and in the supporting Information.

## References

- Allison, S. D. 2006. “Soil Minerals and Humic Acids Alter Enzyme Stability: Implications for Ecosystem Processes.” *Biogeochemistry* 81, no. 3: 361–373. <https://doi.org/10.1007/s10533-006-9046-2>.
- Altenburg, M., H. Machts, and A. Steinhof. 2017. “Sample Preparation at the Jena <sup>14</sup>C Laboratory.” *Radiocarbon* 59, no. 3: 815–830. <https://doi.org/10.1017/RDC.2017.50>.
- Amelung, W., A. Miltner, X. Zhang, and W. Zech. 2001. “Fate of Microbial Residues During Litter Decomposition as Affected by Minerals.” *Soil Science* 166, no. 9: 598–606. <https://doi.org/10.1097/00010694-200109000-00003>.
- Appuhn, A., and R. G. Joergensen. 2006. “Microbial Colonisation of Roots as a Function of Plant Species.” *Soil Biology & Biochemistry* 38, no. 5: 1040–1051. <https://doi.org/10.1016/j.soilbio.2005.09.002>.
- Armstrong McKay, D. I., A. Staal, J. F. Abrams, et al. 2022. “Exceeding 1.5°C Global Warming Could Trigger Multiple Climate Tipping Points.” *Science* 377, no. 6611: eabn7950. <https://doi.org/10.1126/science.abn7950>.
- Behnke, M. I., S. E. Tank, J. W. McClelland, et al. 2023. “Aquatic Biomass is a Major Source to Particulate Organic Matter Export in Large Arctic Rivers.” *Proceedings of the National Academy of Sciences of the United States of America* 120, no. 12: e2209883120. <https://doi.org/10.1073/pnas.2209883120>.
- Blakemore, L. C., P. L. Searle, and B. K. Daly. 1981. *Methods for Chemical Analysis of Soils*. Lower Hutt, New Zealand: Department of Scientific and Industrial Research.
- Broder, T., C. Blodau, H. Biester, and K. H. Knorr. 2012. “Peat Decomposition Records in Three Pristine Ombrotrophic Bogs in Southern Patagonia.” *Biogeosciences* 9, no. 4: 1479–1491. <https://doi.org/10.5194/bg-9-1479-2012>.
- Buckeridge, K. M., C. Creamer, and J. Whitaker. 2022. “Deconstructing the Microbial Necromass Continuum to Inform Soil Carbon Sequestration.” *Functional Ecology* 36, no. 6: 1396–1410. <https://doi.org/10.1111/1365-2435.14014>.
- Buckeridge, K. M., A. F. La Rosa, K. E. Mason, et al. 2020. “Sticky Dead Microbes: Rapid Abiotic Retention of Microbial Necromass in Soil.” *Soil Biology & Biochemistry* 149: 107929. <https://doi.org/10.1016/j.soilbio.2020.107929>.
- Camenzind, T., K. Mason-Jones, I. Mansour, M. C. Rillig, and J. Lehmann. 2023. “Formation of Necromass-Derived Soil Organic

Carbon Determined by Microbial Death Pathways.” *Nature Geoscience* 16, no. 2: 115–122. <https://doi.org/10.1038/s41561-022-01100-3>.

Chang, L., G. Yu, and C. Liu. 2023. “Interfacial Processes and Mechanisms of Synergistic Degradation of Dichlorobiphenyl by White Rot Fungi and Magnetite Nanoparticles.” *Science China Earth Sciences* 66, no. 9: 2057–2065. <https://doi.org/10.1007/s11430-023-1141-x>.

Cotrufo, M. F., and J. M. Lavelle. 2022. “Chapter One - Soil Organic Matter Formation, Persistence, and Functioning: A Synthesis of Current Understanding to Inform Its Conservation and Regeneration.” In *Advances in Agronomy*, edited by D. L. Sparks, vol. 172, 1–66. Amsterdam, The Netherlands: Academic Press.

Cotrufo, M. F., M. D. Wallenstein, C. M. Boot, K. Deneff, and E. Paul. 2013. “The Microbial Efficiency-Matrix Stabilization (MEMS) Framework Integrates Plant Litter Decomposition With Soil Organic Matter Stabilization: Do Labile Plant Inputs Form Stable Soil Organic Matter?” *Global Change Biology* 19, no. 4: 988–995. <https://doi.org/10.1111/gcb.12113>.

Coward, E. K., A. T. Thompson, and A. F. Plante. 2017. “Iron-Mediated Mineralogical Control of Organic Matter Accumulation in Tropical Soils.” *Geoderma* 306: 206–216. <https://doi.org/10.1016/j.geoderma.2017.07.026>.

Crowther, T. W., J. van den Hoogen, J. Wan, et al. 2019. “The Global Soil Community and Its Influence on Biogeochemistry.” *Science* 365, no. 6455: eaav0550. <https://doi.org/10.1126/science.aav0550>.

Dai, X. Y., C. L. Ping, M. E. Hines, X. D. Zhang, and W. Zech. 2002. “Amino Sugars in Arctic Soils.” *Communications in Soil Science and Plant Analysis* 33, no. 5–6: 789–805. <https://doi.org/10.1081/CSS-120003066>.

Darrouzet-Nardi, A., I. S. Asaff, M. Mauritz, et al. 2023. “Consistent Microbial and Nutrient Resource Island Patterns During Monsoon Rain in a Chihuahuan Desert Bajada Shrubland.” *Ecosphere* 14, no. 4: e4475. <https://doi.org/10.1002/ecs2.4475>.

Doetterl, S., A. A. Berhe, C. Arnold, et al. 2018. “Links Among Warming, Carbon and Microbial Dynamics Mediated by Soil Mineral Weathering.” *Nature Geoscience* 11: 589–593. <https://doi.org/10.1038/s41561-018-0168-7>.

Doetterl, S., A. Stevens, J. Six, et al. 2015. “Soil Carbon Storage Controlled by Interactions Between Geochemistry and Climate.” *Nature Geoscience* 8, no. 10: 780–783. <https://doi.org/10.1038/ngeo2516>.

Engelking, B., H. Flessa, and R. G. Joergensen. 2007. “Shifts in Amino Sugar and Ergosterol Contents After Addition of Sucrose and Cellulose to Soil.” *Soil Biology & Biochemistry* 39, no. 8: 2111–2118. <https://doi.org/10.1016/j.soilbio.2007.03.020>.

Flemming, H.-C., and S. Wuertz. 2019. “Bacteria and Archaea on Earth and Their Abundance in Biofilms.” *Nature Reviews Microbiology* 17, no. 4: 247–260. <https://doi.org/10.1038/s41579-019-0158-9>.

García-Palacios, P., M. A. Bradford, I. Benavente-Ferraces, et al. 2024. “Dominance of Particulate Organic Carbon in Top Mineral Soils in Cold Regions.” *Nature Geoscience* 17, no. 2: 145–150. <https://doi.org/10.1038/s41561-023-01354-5>.

Gavazov, K., A. Canarini, V. E. J. Jasey, et al. 2022. “Plant-Microbial Linkages Underpin Carbon Sequestration in Contrasting Mountain Tundra Vegetation Types.” *Soil Biology & Biochemistry* 165: 108530. <https://doi.org/10.1016/j.soilbio.2021.108530>.

Gu, B., J. Schmitt, Z. Chen, L. Liang, and J. F. McCarthy. 1994. “Adsorption and Desorption of Natural Organic Matter on Iron Oxide: Mechanisms and Models.” *Environmental Science & Technology* 28, no. 1: 38–46. <https://doi.org/10.1021/es00050a007>.

Hall, S. J., and W. L. Silver. 2013. “Iron Oxidation Stimulates Organic Matter Decomposition in Humid Tropical Forest Soils.” *Global Change Biology* 19, no. 9: 2804–2813. <https://doi.org/10.1111/gcb.12229>.

- Hall, S. J., C. Ye, S. R. Weintraub, and W. C. Hockaday. 2020. "Molecular Trade-Offs in Soil Organic Carbon Composition at Continental Scale." *Nature Geoscience* 13: 687–692. <https://doi.org/10.1038/s41561-020-0634-x>.
- He, M., K. Fang, L. Chen, et al. 2022. "Depth-Dependent Drivers of Soil Microbial Necromass Carbon Across Tibetan Alpine Grasslands." *Global Change Biology* 28, no. 3: 936–949. <https://doi.org/10.1111/gcb.15969>.
- Heckman, K., C. E. Hicks Pries, C. R. Lawrence, et al. 2022. "Beyond Bulk: Density Fractions Explain Heterogeneity in Global Soil Carbon Abundance and Persistence." *Global Change Biology* 28, no. 3: 1178–1196. <https://doi.org/10.1111/gcb.16023>.
- Hodgkins, S. B., M. M. Tfaily, C. K. McCalley, et al. 2014. "Changes in Peat Chemistry Associated With Permafrost Thaw Increase Greenhouse Gas Production." *Proceedings of the National Academy of Sciences of the United States of America* 111, no. 16: 5819–5824. <https://doi.org/10.1073/pnas.1314641111>.
- Hu, H., C. Qian, K. Xue, et al. 2024. "Reducing the Uncertainty in Estimating Soil Microbial-Derived Carbon Storage." *Proceedings of the National Academy of Sciences of the United States of America* 121, no. 35: e2401916121. <https://doi.org/10.1073/pnas.2401916121>.
- Jackson, R. B., K. Lajtha, S. E. Crow, G. Hugelius, M. G. Kramer, and G. Piñeiro. 2017. "The Ecology of Soil Carbon: Pools, Vulnerabilities, and Biotic and Abiotic Controls." *Annual Review of Ecology, Evolution, and Systematics* 48, no. 1: 419–445. <https://doi.org/10.1146/annurev-ecolsys-112414-054234>.
- Jaworska, H., H. Dąbkowska-Naskręt, and M. Kobierski. 2016. "Iron Oxides as Weathering Indicator and the Origin of Luvisols From the Vistula Glaciation Region in Poland." *Journal of Soils and Sediments* 16, no. 2: 396–404. <https://doi.org/10.1007/s11368-015-1201-8>.
- Jiang, B., D. Duan, L. Gao, et al. 2018. "Standardized Assays for Determining the Catalytic Activity and Kinetics of Peroxidase-Like Nanozymes." *Nature Protocols* 13, no. 7: 1506–1520. <https://doi.org/10.1038/s41596-018-0001-1>.
- Jones, M. E., R. E. LaCroix, J. Zeigler, S. C. Ying, P. S. Nico, and M. Keiluweit. 2020. "Enzymes, Manganese, or Iron? Drivers of Oxidative Organic Matter Decomposition in Soils." *Environmental Science & Technology* 54: 14114–14123. <https://doi.org/10.1021/acs.est.0c04212>.
- Kaiser, K., G. Guggenberger, L. Haumaier, and W. Zech. 1997. "Dissolved Organic Matter Sorption on Sub Soils and Minerals Studied by <sup>13</sup>C NMR and DRIFT Spectroscopy." *European Journal of Soil Science* 48, no. 2: 301–310. <https://doi.org/10.1111/j.1365-2389.1997.tb00550.x>.
- Kang, J., C. Qu, W. Chen, P. Cai, C. Chen, and Q. Huang. 2024. "Organo–Organic Interactions Dominantly Drive Soil Organic Carbon Accrual." *Global Change Biology* 30, no. 1: e17147. <https://doi.org/10.1111/gcb.17147>.
- Kleber, M., K. Eusterhues, M. Keiluweit, C. Mikutta, R. Mikutta, and P. S. Nico. 2015. "Chapter One- Mineral–Organic Associations: Formation, Properties, and Relevance in Soil Environments." In *Advances in Agronomy*, edited by L. S. Donald, vol. 130, 1–140. Amsterdam, The Netherlands: Academic Press.
- Koegel-Knabner, I., G. Guggenberger, M. Kleber, et al. 2008. "Organo–Mineral Associations in Temperate Soils: Integrating Biology, Mineralogy, and Organic Matter Chemistry." *Journal of Plant Nutrition and Soil Science* 171, no. 1: 61–82. <https://doi.org/10.1002/jpln.200700048>.
- Kramer, M. G., and O. A. Chadwick. 2018. "Climate-Driven Thresholds in Reactive Mineral Retention of Soil Carbon at the Global Scale." *Nature Climate Change* 8, no. 12: 1104–1108. <https://doi.org/10.1038/s41558-018-0341-4>.
- Lalonde, K., A. Mucci, A. Ouellet, and Y. Gelin. 2012. "Preservation of Organic Matter in Sediments Promoted by Iron." *Nature* 483, no. 7388: 198–200. <https://doi.org/10.1038/nature10855>.
- Legendre, P. 2007. "Studying Beta Diversity: Ecological Variation Partitioning by Multiple Regression and Canonical Analysis." *Journal of Plant Ecology* 1, no. 1: 3–8. <https://doi.org/10.1093/jpe/rtm001>.
- Lehmann, J., J. Kinyangi, and D. Solomon. 2007. "Organic Matter Stabilization in Soil Microaggregates: Implications From Spatial Heterogeneity of Organic Carbon Contents and Carbon Forms." *Biogeochemistry* 85, no. 1: 45–57. <https://doi.org/10.1007/s10533-007-9105-3>.
- Lenton, T. M., H. Held, E. Kriegler, et al. 2008. "Tipping Elements in the Earth's Climate System." *Proceedings of the National Academy of Sciences of the United States of America* 105, no. 6: 1786–1793. <https://doi.org/10.1073/pnas.0705414105>.
- Liang, C., W. Amelung, J. Lehmann, and M. Kästner. 2019. "Quantitative Assessment of Microbial Necromass Contribution to Soil Organic Matter." *Global Change Biology* 25, no. 11: 3578–3590. <https://doi.org/10.1111/gcb.14781>.
- Luo, Y., M. Xiao, H. Yuan, et al. 2021. "Rice Rhizodeposition Promotes the Build-Up of Organic Carbon in Soil via Fungal Necromass." *Soil Biology & Biochemistry* 160: 108345. <https://doi.org/10.1016/j.soilbio.2021.108345>.
- Martens, J., C. W. Mueller, P. Joshi, et al. 2023. "Stabilization of Mineral-Associated Organic Carbon in Pleistocene Permafrost." *Nature Communications* 14, no. 1: 2120. <https://doi.org/10.1038/s41467-023-37766-5>.
- McGuire, A. D., D. M. Lawrence, C. Koven, et al. 2018. "Dependence of the Evolution of Carbon Dynamics in the Northern Permafrost Region on the Trajectory of Climate Change." *Proceedings of the National Academy of Sciences of the United States of America* 115, no. 15: 3882–3887. <https://doi.org/10.1073/pnas.1719903115>.
- Mehra, O. P., and M. L. Jackson. 1958. "Iron Oxide Removal From Soils and Clays by a Dithionite-Citrate System Buffered With Sodium Bicarbonate." *Clays and Clay Minerals* 7, no. 1: 317–327. <https://doi.org/10.1346/CCMN.1958.0070122>.
- Mikutta, R., S. Turner, A. Schippers, et al. 2019. "Microbial and Abiotic Controls on Mineral-Associated Organic Matter in Soil Profiles Along an Ecosystem Gradient." *Scientific Reports* 9, no. 1: 10294. <https://doi.org/10.1038/s41598-019-46501-4>.
- Page, S. E., G. W. Kling, M. Sander, et al. 2013. "Dark Formation of Hydroxyl Radical in Arctic Soil and Surface Waters." *Environmental Science & Technology* 47, no. 22: 12860–12867. <https://doi.org/10.1021/es4033265>.
- Patzner, M. S., N. Kainz, E. Lundin, et al. 2022. "Seasonal Fluctuations in Iron Cycling in Thawing Permafrost Peatlands." *Environmental Science & Technology* 56, no. 7: 4620–4631. <https://doi.org/10.1021/acs.est.1c06937>.
- Patzner, M. S., M. Logan, A. M. McKenna, et al. 2022. "Microbial Iron Cycling During Palsa Hillslope Collapse Promotes Greenhouse Gas Emissions Before Complete Permafrost Thaw." *Communications Earth & Environment* 3, no. 1: 76. <https://doi.org/10.1038/s43247-022-00407-8>.
- Patzner, M. S., C. W. Mueller, M. Malusova, et al. 2020. "Iron Mineral Dissolution Releases Iron and Associated Organic Carbon During Permafrost Thaw." *Nature Communications* 11, no. 1: 6329. <https://doi.org/10.1038/s41467-020-20102-6>.
- Ping, C. L., J. D. Jastrow, M. T. Jorgenson, G. J. Michaelson, and Y. L. Shur. 2015. "Permafrost Soils and Carbon Cycling." *Soil* 1, no. 1: 147–171. <https://doi.org/10.5194/soil-1-147-2015>.
- Possinger, A. R., M. J. Zachman, A. Enders, et al. 2020. "Organo–Organic and Organo–Mineral Interfaces in Soil at the Nanometer Scale." *Nature Communications* 11, no. 1: 6103. <https://doi.org/10.1038/s41467-020-19792-9>.
- Prater, I., S. Zubrzycki, F. Buegger, et al. 2020. "From Fibrous Plant Residues to Mineral-Associated Organic Carbon—The Fate of Organic

- Matter in Arctic Permafrost Soils." *Biogeosciences* 17, no. 13: 3367–3383. <https://doi.org/10.5194/bg-17-3367-2020>.
- Robert, A., and B. Meunier. 2022. "How to Define a Nanozyme." *ACS Nano* 16, no. 5: 6956–6959. <https://doi.org/10.1021/acsnano.2c02966>.
- Safarik, I., and J. Prochazkova. 2022. "Magnetic Enzyme-Mimetic Minerals With Peroxidase-Like Activity Can Contribute to Measured Soil Peroxidase Activity." *Soil Biology & Biochemistry* 168: 108639. <https://doi.org/10.1016/j.soilbio.2022.108639>.
- Safarik, I., and J. Prochazkova. 2024. "Soil Montmorillonite Can Exhibit Peroxidase-Like Activity." *Clay Minerals* 59, no. 1: 22–25. <https://doi.org/10.1180/clm.2024.3>.
- Satterfield, C. N., and A. H. Bonnell. 1955. "Interferences in Titanium Sulfate Method for Hydrogen Peroxide." *Analytical Chemistry* 27, no. 7: 1174–1175. <https://doi.org/10.1021/ac60103a042>.
- Schuur, E. A. G., B. W. Abbott, R. Commann, et al. 2022. "Permafrost and Climate Change: Carbon Cycle Feedbacks From the Warming Arctic." *Annual Review of Environment and Resources* 47, no. 1: 343–371. <https://doi.org/10.1146/annurev-enviro-012220-011847>.
- Shabtai, I. A., R. C. Wilhelm, S. A. Schweizer, C. Höschen, D. H. Buckley, and J. Lehmann. 2023. "Calcium Promotes Persistent Soil Organic Matter by Altering Microbial Transformation of Plant Litter." *Nature Communications* 14, no. 1: 6609. <https://doi.org/10.1038/s41467-023-42291-6>.
- Sierra, C. A., A. M. Hoyt, Y. He, and S. E. Trumbore. 2018. "Soil Organic Matter Persistence as a Stochastic Process: Age and Transit Time Distributions of Carbon in Soils." *Global Biogeochemical Cycles* 32, no. 10: 1574–1588. <https://doi.org/10.1029/2018GB005950>.
- Sinsabaugh, R. L. 2010. "Phenol Oxidase, Peroxidase and Organic Matter Dynamics of Soil." *Soil Biology & Biochemistry* 42, no. 3: 391–404. <https://doi.org/10.1016/j.soilbio.2009.10.014>.
- Sinsabaugh, R. L., C. L. Lauber, M. N. Weintraub, et al. 2008. "Stoichiometry of Soil Enzyme Activity at Global Scale." *Ecology Letters* 11, no. 11: 1252–1264. <https://doi.org/10.1111/j.1461-0248.2008.01245.x>.
- Sokol, N. W., and M. A. Bradford. 2018. "Microbial Formation of Stable Soil Carbon is More Efficient From Belowground Than Aboveground Input." *Nature Geoscience* 12: 46–53. <https://doi.org/10.1038/s41561-018-0258-6>.
- Stursova, M., and R. L. Sinsabaugh. 2008. "Stabilization of Oxidative Enzymes in Desert Soil May Limit Organic Matter Accumulation." *Soil Biology & Biochemistry* 40, no. 2: 550–553. <https://doi.org/10.1016/j.soilbio.2007.09.002>.
- Sun, F.-S., C. Ma, G.-H. Yu, et al. 2023. "Organic Carbon Preservation in Wetlands: Iron Oxide Protection vs. Thermodynamic Limitation." *Water Research* 241: 120133. <https://doi.org/10.1016/j.watres.2023.120133>.
- Teufel, B., and L. Sushama. 2019. "Abrupt Changes Across the Arctic Permafrost Region Endanger Northern Development." *Nature Climate Change* 9, no. 11: 858–862. <https://doi.org/10.1038/s41558-019-0614-6>.
- Tian, L., and W. Shi. 2014. "Soil Peroxidase Regulates Organic Matter Decomposition Through Improving the Accessibility of Reducing Sugars and Amino Acids." *Biology and Fertility of Soils* 50, no. 5: 785–794. <https://doi.org/10.1007/s00374-014-0903-1>.
- Trusiak, A., L. A. Treibergs, G. W. Kling, and R. M. Cory. 2018. "The Role of Iron and Reactive Oxygen Species in the Production of CO<sub>2</sub> in Arctic Soil Waters." *Geochimica et Cosmochimica Acta* 224: 80–95. <https://doi.org/10.1016/j.gca.2017.12.022>.
- Turetsky, M. R., B. W. Abbott, M. C. Jones, et al. 2020. "Carbon Release Through Abrupt Permafrost Thaw." *Nature Geoscience* 13, no. 2: 138–143. <https://doi.org/10.1038/s41561-019-0526-0>.
- Vogel, C., C. W. Mueller, C. Hoschen, et al. 2014. "Submicron Structures Provide Preferential Spots for Carbon and Nitrogen Sequestration in Soils." *Nature Communications* 5: 2947. <https://doi.org/10.1038/ncomm3947>.
- Wang, C., L. Qu, L. Yang, et al. 2021. "Large-Scale Importance of Microbial Carbon Use Efficiency and Necromass to Soil Organic Carbon." *Global Change Biology* 27, no. 10: 2039–2048. <https://doi.org/10.1111/gcb.15550>.
- Wang, X., C. Wang, X. Fan, et al. 2024. "Mineral Composition Controls the Stabilization of Microbially Derived Carbon and Nitrogen in Soils: Insights From an Isotope Tracing Model." *Global Change Biology* 30, no. 1: e17156. <https://doi.org/10.1111/gcb.17156>.
- Wasner, D., R. Abramoff, M. Griepentrog, E. Z. Venegas, P. Boeckx, and S. Doetterl. 2024. "The Role of Climate, Mineralogy and Stable Aggregates for Soil Organic Carbon Dynamics Along a Geoclimatic Gradient." *Global Biogeochemical Cycles* 38, no. 7: e2023GB007934. <https://doi.org/10.1029/2023GB007934>.
- Weng, Z., L. Van Zwieten, E. Tavakkoli, et al. 2022. "Microspectroscopic Visualization of How Biochar Lifts the Soil Organic Carbon Ceiling." *Nature Communications* 13, no. 1: 5177. <https://doi.org/10.1038/s41467-022-32819-7>.
- Witzgall, K., A. Vidal, D. I. Schubert, et al. 2021. "Particulate Organic Matter as a Functional Soil Component for Persistent Soil Organic Carbon." *Nature Communications* 12, no. 1: 4115. <https://doi.org/10.1038/s41467-021-24192-8>.
- Xiao, K. Q., Y. Zhao, C. Liang, et al. 2023. "Introducing the Soil Mineral Carbon Pump." *Nature Reviews Earth and Environment* 4: 135–136. <https://doi.org/10.1038/s43017-023-00396-y>.
- Xu, L. X., F. Wang, Y. Yao, et al. 2024. "Key Role of Microbial Necromass and Iron Minerals in Retaining Micronutrients and Facilitating Biological Nitrogen Fixation in Paddy Soils." *Fundamental Research*. <https://doi.org/10.1016/j.fmre.2024.02.007>.
- Yu, G.-H., Y. Kuzyakov, Y. Luo, et al. 2021. "Molybdenum Bioavailability and Asymbiotic Nitrogen Fixation in Soils Are Raised by Iron (Oxyhydr) oxide-Mediated Free Radical Production." *Environmental Science & Technology* 55, no. 21: 14979–14989. <https://doi.org/10.1021/acs.est.1c04240>.
- Zandieh, M., and J. Liu. 2021. "Nanozyme Catalytic Turnover and Self-Limited Reactions." *ACS Nano* 15, no. 10: 15645–15655. <https://doi.org/10.1021/acsnano.1c07520>.
- Zhang, R., L. Chen, Q. Liang, et al. 2021. "Unveiling the Active Sites on Ferrihydrite With Apparent Catalase-Like Activity for Potentiating Radiotherapy." *Nano Today* 41: 101317. <https://doi.org/10.1016/j.nantod.2021.101317>.

## Supporting Information

Additional supporting information can be found online in the Supporting Information section.